

Cobalt Nanoparticle Langmuir–Schaefer Films on Ethylene Glycol Subphase

Elina Pohjalainen,[†] Maija Pohjakallio,[†] Christoffer Johans,^{*†} Kyösti Kontturi,[†] Jaakko V. I. Timonen,[‡] Olli Ikkala,[‡] Robin H. A. Ras,[‡] Tapani Viitala,[§] Markku T. Heino,[⊥] and Eira T. Seppälä[⊥]

[†]Department of Chemistry, Aalto University, P.O.B. 16100, FI-00076 Aalto, Finland, [‡]Molecular Materials, Department of Applied Physics, Helsinki University of Technology/Aalto University, Puumiehenkuja 2, FI-02150 Espoo, Finland, [§]KSV Instruments, Höylämötie 7, 00380 Helsinki, Finland, and [⊥]Nokia Research Center, Itämerenkatu 11-13, FI-00180 Helsinki, Finland

Received April 23, 2010. Revised Manuscript Received June 3, 2010

The Langmuir–Schaefer (LS) technique was applied to prepare two-dimensional films of tridodecylamine (TDA)-stabilized Co nanoparticles. Ethylene glycol was used as the subphase because the Co nanoparticles spread better on it than on water. Surface pressure–area isotherms provided very little information on the floating films, and Brewster angle microscopy (BAM) was needed to characterize the film formation *in situ*. In addition to the subphase, various other experimental factors were tested in the LS film preparation, including solvent and presence of free TDA ligands and poly(styrene-*b*-ethylene oxide) (PS-*b*-PEO) in the nanoparticle dispersion. LS films deposited from dispersions from which the excess TDA ligands had been removed by washing the Co nanoparticles with 2-propanol consisted of hexagonally organized particles in rafts that were organized in necklace structures. The addition of PS-*b*-PEO to the deposition dispersion resulted in small nanoparticle rafts evenly distributed over the substrate surface. The best Co-nanoparticle–PS-*b*-PEO films were obtained with a mass ratio of 20:1 between Co (9 nm) and block copolymer (38 200 g/mol, PEO content 22 mass %). These films were successfully transferred onto Formvar-coated TEM grids and characterized by transmission electron microscopy (TEM) and a superconducting quantum interference device (SQUID) magnetometer. At room temperature the films showed superparamagnetic behavior with a saturation magnetization M_s of 100 emu/g (Co). Our work indicates that it is possible to obtain thin superparamagnetic LS films of TDA-stabilized Co nanoparticles. This is an important result as the TDA-stabilized Co nanoparticles show a very good resistance to corrosion.

1. Introduction

Magnetic nanoparticles have gained considerable interest during recent years. In the number of publications, cobalt ranks next to iron and iron oxide.¹ The finite size and high surface area of magnetic nanoparticles give rise to unique properties which make them extremely interesting for many applications such as ferrofluids,² data storage,^{3,4} biotechnology and medicine,^{5,6} antennae,^{7,8} and catalysts.^{9,10} Many of these applications require particles with narrow size distribution in ordered arrays. Because of particle–particle interactions, assemblies of magnetic nanoparticles show features different from both bulk ferromagnets and isolated nanoparticles.^{11–13} A considerable number of studies have been

devoted to preparing two- and three-dimensional nanoparticle superstructures by various methods, such as self-assembly,¹³ spin-coating,¹⁴ layer-by-layer deposition,¹⁵ and Langmuir–Blodgett (LB) and Langmuir–Schaefer (LS) techniques.^{12,16–30}

Langmuir–Blodgett and Langmuir–Schaefer techniques were developed in the 1920s and 1930s, thus long before the burst of

*To whom correspondence should be addressed: e-mail cjhans@cc.hut.fi; Ph +358 9 470 22586; Fax +358 9 470 22580.

- (1) Gubin, S. P.; Koksharov, Y. A. *Inorg. Mater.* **2002**, *38*, 1085.
- (2) Ziolo, R. F.; Giannelis, E. P.; Weinstein, B.; O'Horo, M. P.; Ganguly, B. N.; Mehrotra, V.; Russell, M. W.; Huffman, D. R. *Science* **1992**, *257*, 219.
- (3) Speliotis, D. E. *J. Magn. Mater.* **1999**, *193*, 29.
- (4) Hyeon, T. *Chem. Commun.* **2003**, 927.
- (5) Roger, J.; Pons, J. N.; Massart, R.; Halbreich, A.; Bacri, J. C. *Eur. Phys. J.: Appl. Phys.* **1999**, *5*, 321.
- (6) Gupta, A. K.; Gupta, M. *Biomaterials* **2005**, *26*, 3995.
- (7) Wu, M.; Zhang, Y. D.; Hui, S.; Xiao, T. D.; Shihui, G.; Hines, W. A.; Budnick, J. I.; Yacaman, M. J. *J. Appl. Phys.* **2002**, *92*, 6809.
- (8) Raj, P. M.; Muthana, P.; Xiao, T. D.; Wan, L.; Balaraman, D.; Abothu, I. R.; Bhattacharya, S.; Swaminathan, M.; Tummala, R. *IEEE Adv. Packag. Mater.: Processes, Prop. Interfaces* **2005**, 272.
- (9) Tsang, S. C.; Caps, V.; Paraskevas, I.; Chadwick, D.; Thompson, D. *Angew. Chem.* **2004**, *116*, 5763.
- (10) Lu, A.-H.; Schmidt, W.; Matoussevitch, N.; Bönnermann, H.; Spliethoff, B.; Tesche, B.; Bill, E.; Kiefer, W.; Schuth, F. *Angew. Chem.* **2004**, *116*, 4403.
- (11) Leslie-Pelecky, D. L.; Rieke, R. D. *Chem. Mater.* **1996**, *8*, 1770–1783.
- (12) Poddar, P.; Telem-Sharif, T.; Fried, T.; Markovich, G. *Phys. Rev. B* **2002**, *66*, 060403.
- (13) Legrand, J.; Petit, C.; Bazin, D.; Pileni, M. P. *Appl. Surf. Sci.* **2000**, *164*, 186.

- (14) Hong, Y.-K.; Kim, H.; Lee, G.; Kim, W.; Park, J.; Cheon, J.; Koo, J.-Y. *Appl. Phys. Lett.* **2002**, *80*, 844.

- (15) Sun, S.; Anders, S.; Hamann, H. F.; Thiele, J.-U.; Baglin, J. E. E.; Thompson, T.; Fullerton, E. E.; Murray, C. B.; Terris, B. D. *J. Am. Chem. Soc.* **2002**, *124*, 2884.
- (16) Aleksandrovic, V.; Greshnykh, D.; Randjelovic, I.; Frömsdorf, A.; Kornowski, A.; Roth, S. V.; Klinker, C.; Weller, H. *ACS Nano* **2008**, *2*(6), 1123–1130.
- (17) Fried, T.; Shemer, G.; Markovich, G. *Adv. Mater.* **2001**, *13*, 1158–1161.
- (18) Telem-Sharif, T.; Markovich, G. *J. Chem. Phys.* **2005**, *123*, 204745.
- (19) Parvin, S.; Matsui, J.; Sato, E.; Miyashita, T. *J. Colloid Interface Sci.* **2007**, *313*, 128–134.
- (20) Lee, D. K.; Kim, Y. H.; Kim, C. W.; Cha, H. G.; Kang, Y. S. *J. Phys. Chem. B* **2007**, *111*, 9288–9293.
- (21) Sachan, M.; Walrath, N. D.; Majetich, S. A.; Krycka, K.; Kao, C.-C. *J. Appl. Phys.* **2006**, *99*, 08C302.
- (22) Majetich, S. A.; Sachan, M.; Kan, S.; Cheng, Y.; Gardener, J. *Mater. Res. Soc. Symp. Proc.* **2005**, *877E*, S4.3.1.
- (23) Park, J.-I.; Lee, W.-R.; Bae, S.-S.; Kim, Y. J.; Yoo, K.-H.; Cheon, J.; Kim, S. *J. Phys. Chem. B* **2005**, *109*, 13119–13123.
- (24) Lefebvre, S.; Ménager, C.; Cabuil, V.; Assenheimer, M.; Gallet, F.; Flament, C. *J. Phys. Chem. B* **1998**, *102*, 2733–2738.
- (25) Meldrum, F. C.; Kotov, N. A.; Fendler, J. H. *J. Phys. Chem.* **1994**, *98*, 4506–4510.
- (26) Mammeri, F.; Le Bras, Y.; Daou, T. J.; Gallani, J.-L.; Colis, S.; Pourroy, G.; Donnio, B.; Guillon, D.; Begin-Colin, S. *J. Phys. Chem. B* **2009**, *113*, 734–738.
- (27) Knobel, M.; Nunes, W. C.; Winnischofer, H.; Rocha, T. C. R.; Socolovsky, L. M.; Mayorga, C. L.; Zanchet, D. *J. Non-Cryst. Solids* **2007**, *353*, 743–747.
- (28) Guo, Q.; Teng, X.; Rahman, S.; Yang, H. *J. Am. Chem. Soc.* **2003**, *125*, 630–631.
- (29) Iakovenko, S. A.; Trifonov, A. S.; Giersig, M.; Mamedov, A.; Nagesha, D. K.; Hanin, V. V.; Soldatov, E. C.; Kotov, N. A. *Adv. Mater.* **1999**, *11*, 388–392.
- (30) Li, H.; Sachsenhofer, R.; Binder, W. H.; Henze, T.; Thurn-Albrecht, T.; Busse, K.; Kressler, J. *Langmuir* **2009**, *25*, 8320–8329.

nanoscience and nanotechnology. Though originally designed for the formation of monolayers of amphiphilic molecules, the methods are nowadays also used for preparing ordered structures of other materials including hydrophobic particles. In addition to metallic nanoparticles, LS films of e.g. polystyrene^{31,32} and fullerenes³³ have been prepared. As LB and LS techniques are based on the formation of a layer at an air–liquid interface, they provide one considerable advantage over many other thin film formation techniques: the liquid surface is always ideally smooth. Thus, no industrious pretreatments of the surface are needed, and the liquid substrate onto which the film is formed can be considered to be repeatedly the same. Floating films do not have as many applications as films on solid surfaces, and the floating Langmuir films are often transferred onto solid substrates by dipping a solid substrate through the floating film vertically (in LB) or horizontally (in LS). Our interest in Langmuir films of magnetic particles stems from the possibility to adjust the distance between particles and thus tailor the magnetic properties of particle assemblies.

Because of strong particle–particle interactions and the hydrophobic nature of the surfactant-stabilized nanoparticles, the preparation of good quality LS and LB layers of magnetic nanoparticles is not trivial. However, by careful optimization of experimental conditions, homogeneous LS and LB layers have been obtained. Among magnetic nanoparticles, iron oxide particles Fe₃O₄^{12,18–20,26,27} and Fe₂O₃^{24,28–30} are the most studied LS and LB systems. Few LS and LB studies on cobalt alloy nanoparticles,^{16,17,34,35} Fe–Pt nanoparticles,^{36–38} and Ni nanoparticles³⁹ have been reported. Two groups have successfully prepared LS or LB films of Co nanoparticles: Park et al.²³ using tetradecanoic acid and sodium bis(ethylhexyl) sulfosuccinate-protected particles (10 nm) on water subphases and Sachan et al.^{21,22} using oleic acid-protected particles (7–8 nm) on ethylene glycol subphases.

Most of the LS and LB studies on magnetic nanoparticles are performed with particles with an organic shell containing long chain carboxylic acid molecules. In many applications the organic shell plays a vital role, and the use of other molecules than carboxylic acids may be required. It is thus important to gain information on the LS behavior of magnetic nanoparticles with different types of ligand shells. In this study, we used the Langmuir–Schaefer technique to prepare 2D structures of cobalt nanoparticles stabilized by tridodecylamine (TDA) ligands. TDA molecules are especially interesting ligands as oxidation studies show that TDA protects the Co nanoparticles from oxidation much better than long chain carboxylic acids (see Supporting Information section S1). The aim was to obtain thin magnetic films suitable for RF applications. Various experimental factors were tested, including the nature of the subphase, nature of the solvent in the deposition solution, and washing procedure of the nanoparticle synthesis solution. In addition, the presence of free TDA ligands and diblock copolymer poly(styrene-*b*-ethylene oxide) (PS-*b*-PEO) in the deposition dispersion was investigated. Addition of PS-*b*-PEO increased the

spreading of Co nanoparticles onto the subphase and reduced particle aggregation. Despite several steps in the preparation procedure including washing, precipitation, redispersion, and deposition of the Co nanoparticles onto the subphase–air interface, magnetic characterization indicated that the Co nanoparticles in the PS-*b*-PEO films remained superparamagnetic at room temperature.

In our study, we used ethylene glycol as the subphase because it provided better spreading of the Co nanoparticles than water. As there is a growing interest in obtaining ordered structures of metallic nanoparticles and other new types of materials, it is evident that more information on the Langmuir film formation of nonamphiphilic particles on nonaqueous surfaces is needed.

2. Experimental Section

Co nanoparticles were synthesized by a pressure drop-induced decomposition method.^{40,41} In this method, 2 g of Co₂(CO)₈ is heated together with TDA ligands and dodecane solvent in a reactor under high CO pressure to 170 °C, and then decomposed by applying a rapid pressure drop. The pressure drop is a direct means to control the nucleation rate and thus the particle size, and consequently the synthesis batches were of good quality with a narrow size distribution. The formation of a nanoparticle Langmuir film is highly dependent on the size and other properties of the particles, hence particles from the same synthesis batch were used when drawing conclusions on the influence of the experimental factors. The crystal structure of the particles was multicrystalline fcc.⁴⁰ After the synthesis, the Co nanoparticles were precipitated with 2-propanol to remove excess TDA ligands. The particles were then redispersed in hexane or toluene. The particle concentration was determined from the amount of cobalt in the sample (AAS) and particle size obtained with TEM.

The washing procedure and solvent exchange of the Co nanoparticle synthesis solution must be carried out carefully. In this work, we tried two different procedures: washing and precipitation with ethanol and with 2-propanol. When polar solvent is added into the dodecane synthesis dispersion, the Co nanoparticles precipitate and the solvent can easily be changed. TEM images recorded after the washing and redispersion are presented in the Supporting Information (Figure S2). Ethanol causes aggregation of the TDA-protected Co nanoparticles while washing with 2-propanol leaves the particles intact. Co nanoparticles washed with 2-propanol were easily redispersed in hexane or toluene after washing, whereas the Co nanoparticles washed with ethanol did not redisperse easily but tended to aggregate.

LS films of Co nanoparticles were prepared with a KSV minitrough (KSV Instruments Ltd.) under ambient conditions. Ethylene glycol (99.5%, Merck KGaA) or Milli-Q water was used as the subphase. The subphase temperature was set to 21 °C. Water absorption had a negligible effect on the surface pressure of ethylene glycol subphase during the time scale of the experiment (see Figure S3, Supporting Information). The deposition solution (2–20 mg/mL) was spread on the air–liquid interface by a Hamilton syringe. After spreading, the solvent was let to evaporate and the film to equilibrate for 15 min prior to compression. The films were compressed at 5 mm/min to the desired mean particle area. The mean particle area is calculated from the estimated number of Co nanoparticles divided by the area of the trough and does not consider other components of the film. After the desired compression was reached, the monolayer was let to stabilize for 15 min before transferring it horizontally (Langmuir–Schaefer) onto a Formvar-carbon-coated copper TEM grid (Electron Microscopy Sciences) using a dipper operated at 1 mm/min.

Diblock copolymer poly(styrene-*b*-ethylene oxide) (PS-*b*-PEO) (Polymer Source Inc.) was used to aid the spreading of the

(31) Kumaki, J. *Macromolecules* **1986**, *19*, 2258–2263.

(32) Kumaki, J. *Macromolecules* **1988**, *21*, 749–755.

(33) Miura, Y. F.; Urushibata, M.; Matsuoka, I.; Morita, S.-I.; Sugi, M. *Colloids Surf., A* **2006**, *284–285*, 93–96.

(34) Lee, D. K.; Kang, Y. S. *Colloids Surf., A* **2005**, *257–258*, 237–241.

(35) Lee, D. K.; Kim, Y. H.; Kang, Y. S.; Stroeve, P. J. *Phys. Chem. B* **2005**, *109*, 14939–14944.

(36) Kuroishi, K.; Chen, M.-P.; Kitamono, Y.; Seki, T. *Electrochim. Acta* **2005**, *51*, 867–869.

(37) Guo, Q.; Teng, X.; Yang, H. *Adv. Mater.* **2004**, *16*(15), 1337–1341.

(38) Wang, Y.; Ding, B.; Li, H.; Zhang, X.; Cai, B.; Zhang, Y. *J. Magn. Magn. Mater.* **2007**, *308*, 108–115.

(39) Khomutov, G. B.; Bykov, I. V.; Gainutdinov, R. V.; Polyakov, S. N.; Sergey-Cherenkov, A. N.; Tolstikhina, A. L. *Colloids Surf., A* **2002**, *198–200*, 559–567.

(40) Johans, C.; Pohjakallio, M.; Ijäs, M.; Ge, Y.; Kontturi, K. *Colloids Surf., A* **2008**, *330*, 14–20.

(41) Huuppola, M.; Nguyet, D.; Kontturi, K.; Johans, C. *J. Colloid Interface Sci.* **2010**, *344*, 292–297.

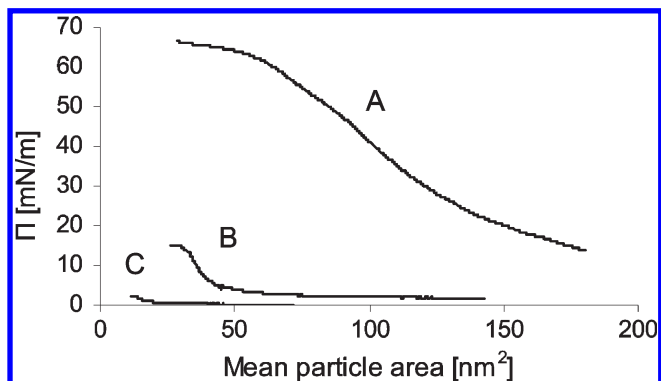


Figure 1. Surface pressure isotherms of (A) nonwashed Co nanoparticles (spread from dodecane) on water, (B) nonwashed Co nanoparticles (spread from dodecane) on ethylene glycol, and (C) washed Co nanoparticles (spread from hexane) on ethylene glycol.

particles. The characteristics of the polymer were molar weight 38 200 g/mol, PEO content 22.0%, and M_w/M_n 1.03. A stock solution of polymer (0.5 mg/mL in chloroform, 99.0–99.4%, Riedel-de Haën) was mixed with the Co nanoparticle dispersion before spreading the mixture on the air–liquid interface.

Brewster angle microscopy (BAM) images were recorded *in situ* with a BAM 300 microscope (KSV Instruments Ltd.). Transmission electron microscope (TEM) measurements were performed with a Tecnai 12 instrument operated at 120 kV accelerating voltage. Magnetization curves were measured with a superconducting quantum interference device (SQUID) magnetometer (Quantum Design, MPMS XL 7) at 293 and 2 K. The grid was aligned in the direction of the magnetic field. The magnetic response of the Formvar-coated carbon TEM grids was subtracted from the sample measurements.

3. Results and Discussion

Our first approach in LS film preparation was to use the as-prepared cobalt nanoparticle dodecane dispersion without additional washing as a small amount of excess ligands has shown to improve the dispersion of magnetic nanoparticles at the air–water interface.^{17,20} The surface pressure–area isotherms of the Co nanoparticles spread from the dodecane dispersion onto water and ethylene glycol are presented in Figure 1. On water, the surface pressure is quite high already at the beginning of the measurement and starts to rise further when the mean particle area is compressed to about 150 nm²/particle. Close to 70 nm²/particle the surface pressure reaches a plateau. Despite the rise in surface pressure TEM images of samples transferred horizontally from the subphase onto TEM grids at 20 mN/m indicated no or very poor film formation. Aggregation and sinking of the Co nanoparticles into the water subphase was also visible, which was attributed to competitive TDA film formation at the air–water interface. (Isotherms of pure TDA on water and ethylene glycol subphases are available in the Supporting Information, Figure S4.) The corresponding rise in surface pressure was also attributed to the excess TDA ligands present in the dodecane dispersion.

We noticed that the nonwashed Co nanoparticles spread better on ethylene glycol than on water, but considerably lower surface pressure values were measured on ethylene glycol compared to those measured on water (Figure 1A,B). On ethylene glycol, the surface pressure starts to increase at ~ 50 nm² where the mean particle area is already smaller than the calculated cross-sectional area of one nanoparticle (71 nm²/particle for 9.5 nm particles). It should be noted that the mean particle area is an estimate that does not account for loss of particles due to possible aggregation and sinking of particles and thus may be significantly smaller than

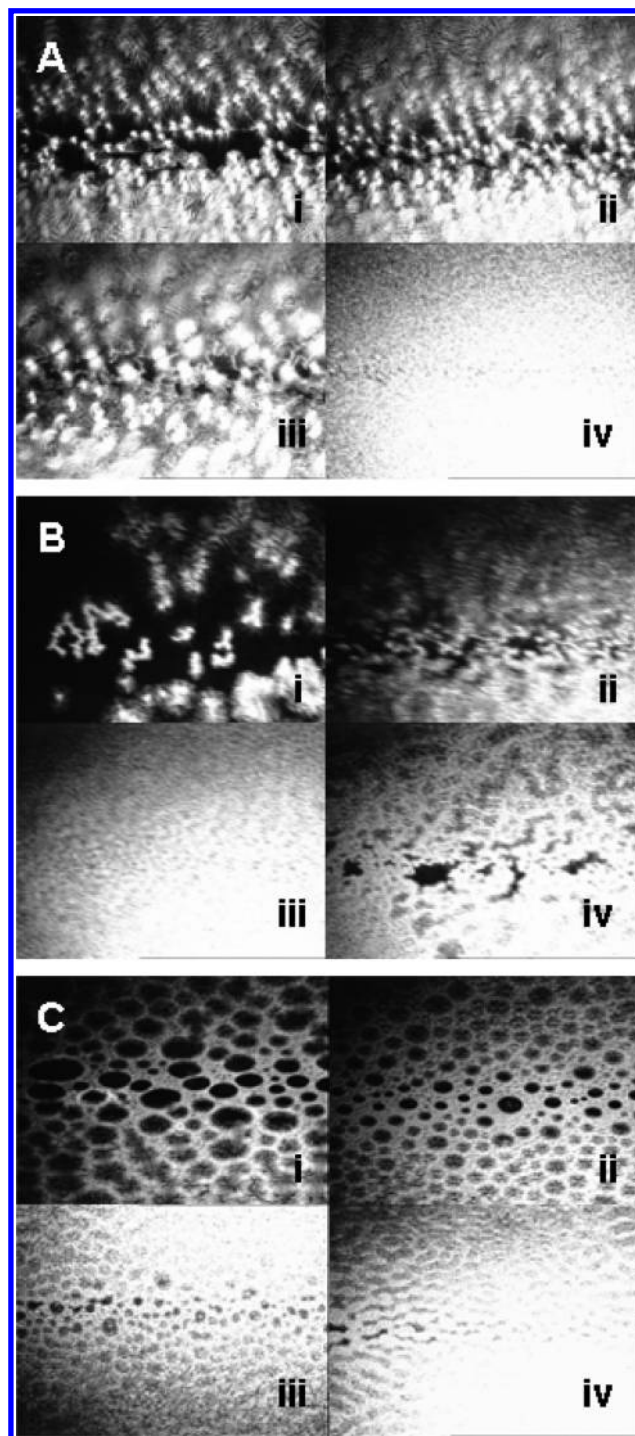


Figure 2. BAM images of floating Langmuir Co nanoparticle films on an ethylene glycol subphase: (A) nonwashed Co nanoparticles spread from dodecane, (B) washed Co nanoparticles spread from hexane, and (C) washed Co nanoparticles spread from toluene. Compression of barriers increases in the order i \rightarrow ii \rightarrow iii \rightarrow iv. Despite the compression, the surface pressure value stayed close to zero in all measurements. The size of the images are $400 \times 300 \mu\text{m}^2$. BAM images of pure TDA are shown in Figure S5 of the Supporting Information.

the true area per particle. The BAM images in Figure 2A reveal that there is film formation on the subphase already before the surface pressure value starts to rise. In BAM the black areas correspond to areas similar to the reference state, i.e., particle-free areas. It can be seen that the particles aggregate into irregular

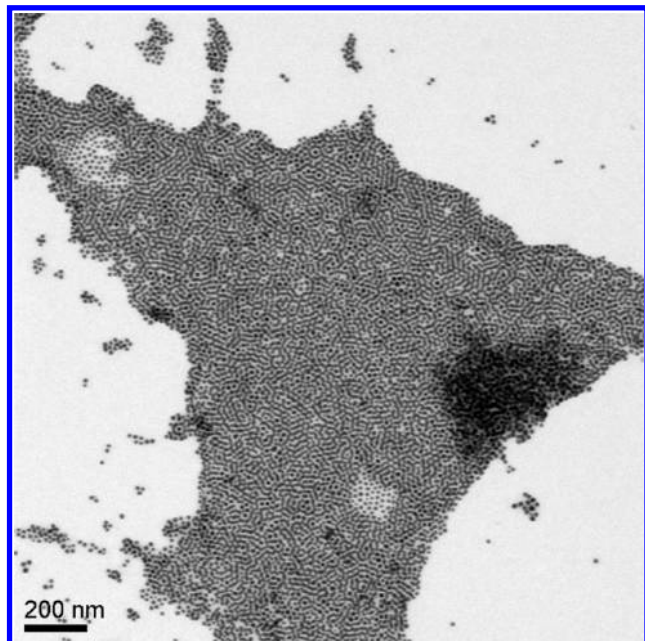


Figure 3. TEM image showing the Co nanoparticle bi- and multi-layer structures formed during Langmuir film formation. The sample is a LS film prepared from nonwashed Co nanoparticles on an ethylene glycol subphase.

domains (white areas) and that the empty area decreases as the film is compressed. This highlights the fact that in this kind of nontraditional system where nonamphiphilic magnetic nanoparticles are deposited on a liquid surface the nature of the surface pressure isotherms is very different from that of amphiphilic molecules on a water subphase. Because of attractive interactions, the Co nanoparticles do not spread evenly over the whole subphase surface (Figure 2A–C) but form islands already at the beginning of the measurement. Thus, we do not see changes in surface pressure before the island have been compressed together. When the film is further compressed, multilayer structures are observed before a substantial increase in the surface pressure (Figure 3). In our system, the surface pressure isotherms gave very little information on the floating Co nanoparticle film. Thus, the surface pressure could not be used as an indicator of the state of the film. Consequently, the transfer of the floating films onto solid TEM grids was performed at a constant mean particle area and not at a constant surface pressure value as traditionally.

The observations clearly indicate that tridodecylamine-protected Co particles spread better on an ethylene glycol–air interface than on a water–air interface, and thus ethylene glycol was used as the subphase in further LS experiments. One reason is the unfavorable contact between water ($\epsilon_r = 80.10$) and the hydrophobic alkyl chains of TDA-stabilized Co nanoparticles. Ethylene glycol is less polar ($\epsilon_r = 41.40$)¹⁶ and thus favors spreading. Another difference between water and ethylene glycol is the surface tension which is much higher for water (71.97 mN/m) than for ethylene glycol (47.99 mN/m).⁴²

To study the effect of excess TDA ligands on Langmuir film formation, the as-synthesized Co nanoparticles were washed with 2-propanol. We could visually observe that removing excess TDA ligands by washing the nanoparticles before deposition on the subphase surface improved the surface coverage. The surface pressure isotherm of the washed particles presented in Figure 1C

shows only a marginal rise in surface pressure, but the BAM images in Figure 2B,C indicate film formation. Because the free TDA ligands are amphiphilic in nature, excess ligands in deposition solution are likely to occupy part of the subphase surface which results in poor nanoparticle coverage. Similar results have been obtained by Aleksandrovic et al.¹⁶ in LS deposition of adamantanecarboxylic acid and hexadecylamine-protected Pt–Co nanoparticle films. Interestingly, some groups suggest that adding a small amount of oleic or stearic acid ligands to the nanoparticle solution helps the spreading of magnetic nanoparticles on a water subphase and thus enhances the quality of the resulting film.^{17,20} Kuroishi et al.³⁶ have used long saturated fatty acid molecules $C_xH_{2x}O_2$ ($x \geq 14$) as a buffer layer between a Fe–Pt nanoparticle film and water. They obtained regular arrangements of the nanoparticles. Evidently, the role of surfactant in the formation of a nanoparticle film is ambiguous and very system dependent. It seems that a small excess of long chain fatty acid molecules may enhance the film quality, but if bulkier ligands like TDA or adamantanecarboxylic acid are used, the removal of excess ligands is crucial in order to obtain LS films with good particle coverage.

The mechanism of Langmuir film formation of TDA-stabilized Co nanoparticles seems to be the same as that reported for many other nanoparticles, e.g., for Fe_3O_4 ,²⁵ $CoFe_2O_4$,³⁵ and Au.⁴³ As shown in Figure 2A–C, the Co nanoparticles do not spread evenly over the whole subphase surface but form domains already at the beginning of the measurement which unite during the compression of the barriers. The TEM image in Figure 3 reveals that the domains consist of bi- or multilayer structures already before a full close-packed monolayer has been formed. Multilayer structures in nanoparticle LS films have been discussed e.g. by Heriot et al.^{44,45} They observed 3-dimensional structures in LS films of 4-methylbenzenethiol-stabilized Au nanoparticles and explained this by a localized film collapse taking place during film transfer onto a solid substrate. In our Co nanoparticle system we have observed darker areas on the subphase surface which we believe are bi- and multilayer structures formed already in the floating Langmuir film before the transfer step.

Figure 2B,C indicates that the washed Co particles spread from hexane and toluene both form domains in the early stages of compression, but that the shape of these domains is different. Co nanoparticles spread from hexane form discrete islands or aggregates that unite upon compression. Particles spread from toluene dispersion form a continuous film with well-defined holes with a diameter in the 10–60 μm range (Figure 2C). The reason for the formation of the holes in the film is unknown. We believe that they are trapped in the film when the solvent (toluene) from the deposition dispersion is evaporated. It is also evident that the size of the holes decreases as the film is compressed.

In the case of drop-casted nanoparticle films, the evaporation rate of the solvent is an important factor in the self-assembly of the particles on the solid substrate, but in the case of Langmuir films the effect of solvent is not as clear. Differences in boiling points (68.7 °C for hexane and 110.6 °C for toluene)⁴² affect the evaporation rate of the solvent and thus also the assembling of the particles at the beginning of the measurement. It has been reported that for alkanethiol-protected gold particles the use of solvent with faster evaporation rate (chloroform) resulted in better quality LS films,⁴⁴ but for lauric acid-stabilized Fe_3O_4

(43) Huang, S.; Tsutsui, G.; Sakaue, H.; Shingubara, S.; Takahagi, T. *J. Vac. Sci. Technol. B* **2001**, *19* (1), 115–120; *19* (6), 2045–2049.

(44) Heriot, S. Y.; Zhang, H.-L.; Evans, S. D.; Richardson, T. H. *Colloids Surf., A* **2006**, *278*, 98–105.

(45) Heriot, S. Y.; Pedrosa, J.-M.; Camacho, L.; Richardson, T. H. *Mater. Sci. Eng., C* **2006**, *26*, 154–162.

(42) Lide, D. R. *CRC Handbook of Chemistry and Physics*, 75th ed.; CRC Press: Boca Raton, FL, 1994.

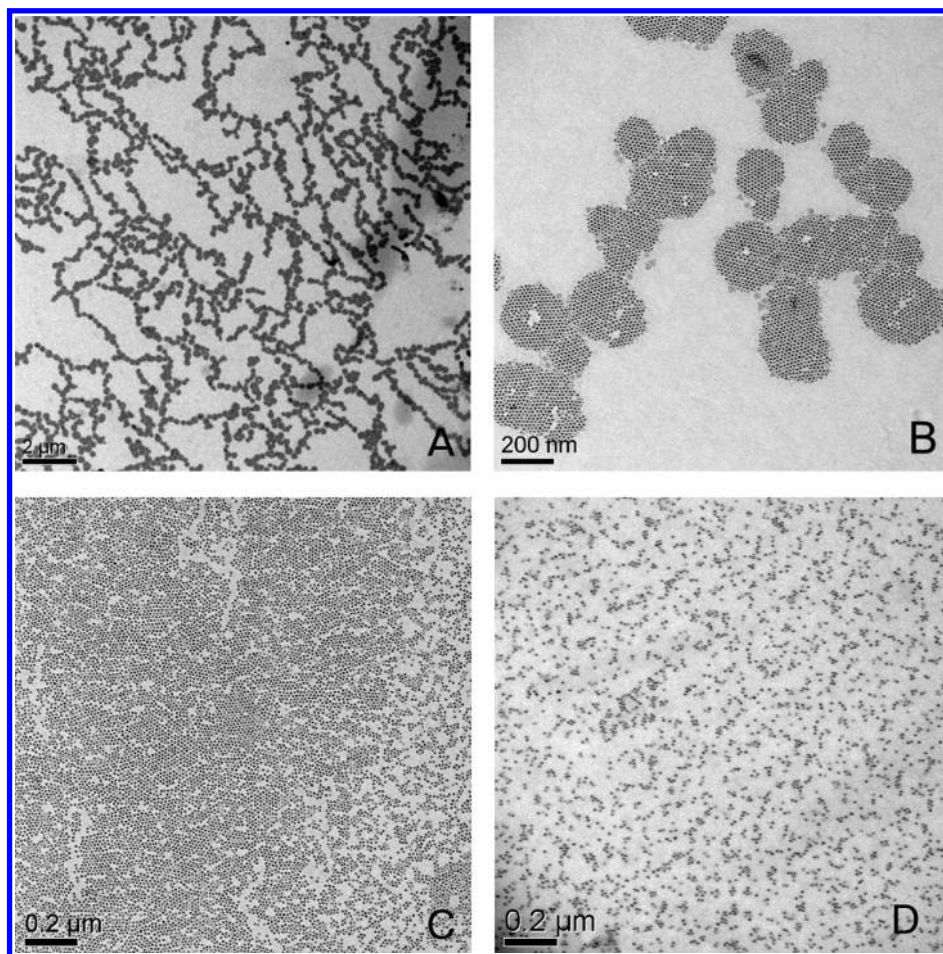


Figure 4. TEM images of Co nanoparticle LS films prepared from washed Co nanoparticles in hexane (A, B) and toluene (C, D) on ethylene glycol. (A) shows the formation of chains of circular particle domains, and (B) shows the hexagonal arrangement of particles within the domains. (C) and (D) indicate the inhomogeneous distribution of the particles in films spread from toluene.

particles deposition using hexane dispersion yielded more uniform films than deposition using chloroform dispersions.²⁵ At room temperature surface tension values for hexane and toluene are 17.9 and 27.9 mN/m.⁴² Surface tension of the solvent affects spreading of the nanoparticle solution on the subphase since the spreading coefficient is dependent on surface tension.⁴⁶

TEM images in Figure 4 reveal differences in the Co nanoparticle LS films deposited from hexane and toluene. Films prepared from hexane dispersion are shown in Figures 4A,B. Circular rafts of ~ 200 particles that organize into long branched chains (necklace structures) are clearly visible in the TEM images. Figures 4A,B correspond to BAM images in Figure 2B, but it should be pointed out that these TEM and BAM images give information on rather different scales.

The Co particles inside the circular domains in Figures 4A,B are packed regularly in a two-dimensional hexagonal pattern. Long spontaneously formed chains are commonly observed for individual nanoparticles provided that the interacting forces between the particles are suitably balanced. If the particles are too weakly magnetic, or the surfactants are too long and bulky, the particles would not magnetically attract each other, which would result in a hexagonal lattice. If the particles are too magnetic or the surfactants too small, the particles would quickly agglomerate into three-dimensional structures. Formation of such chain structures of circular

two-dimensional Co nanoparticle rafts is very interesting and requires a delicate balance of the interaction on two different scales. First, the magnetic interaction between the particles must be weaker than the van der Waals forces for the particles to assemble in a hexagonal pattern in the rafts. However, the magnetic interaction between the particles must be strong enough to give the rafts a magnetic dipole that results in the dipolar raft–raft interactions responsible for the formation of the necklace structures. Same types of necklace structures have been observed by Lee et al.^{34,35} during the formation of Langmuir films of oleic acid-coated CoFe_2O_4 nanoparticles (9.5 ± 1.3 nm in diameter) at the air–water interface.

Figures 4C,D show that if the films are spread from toluene, the distribution of Co nanoparticles is not homogeneous over the substrate surface: in some areas the substrate is almost completely covered whereas in other parts the particles are far from each other or the surface is almost empty. This is especially observed in the upper part of Figure 4C. The TEM images in Figures 4C,D correspond to BAM images in Figure 2C. The holes observed in the BAM images were not detected by TEM. However, it should be remembered that the dimensions of these holes are greater than the scale in our TEM analysis. Interestingly, the two groups who have reported a successful preparation of Co nanoparticle LS films have used toluene dispersions in deposition of the films onto ethylene glycol and water subphases.^{21–23} Their Co nanoparticles were protected by tetradecanoic acid (sodium bis(ethylhexyl) sulfosuccinate) and oleic acid (triethylphosphine) ligands, which can explain the differences. It can thus be concluded that the spreading and organization

(46) Adamson, W. A.; Gast, A. P. *Physical Chemistry of Surfaces*, 6th ed.; Wiley: New York, 1997; pp 101–168.

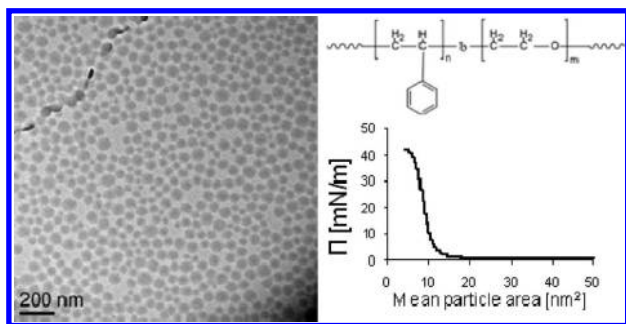


Figure 5. TEM image of a LS film of PS-*b*-PEO prepared on an ethylene glycol subphase at a surface pressure of 25 mN/m and the corresponding surface pressure–area isotherm. The spreading solvent was chloroform. The structure of PS-*b*-PEO is shown above the surface pressure graph.

of the Co nanoparticles on the subphase is a complex interplay of many factors, including the solvent–subphase, nanoparticle–solvent, and nanoparticle–subphase interactions. In the latter two the role of the protecting ligands is crucial.

The aim of the study was to obtain compact magnetic films with potential use in RF applications. To achieve this, a small amount of diblock copolymer PS-*b*-PEO was mixed in the Co nanoparticle–hexane deposition dispersion to aid the spreading of the Co nanoparticles on the subphase. The presence of PS-*b*-PEO was also thought to decrease the possibility of nanoparticle aggregation and to improve the mechanical properties of the film. Several groups have used amphiphilic molecules to improve the dispersion and spreading of hydrophobic molecules on water. For example, poly(ϵ -caprolactone)–polystyrene (PCL–PS),⁴⁷ poly(dimethylsiloxane)–polyhedral oligomeric silsesquioxane,⁴⁸ PS–CdS nanoparticle–PS-*b*-PEO,⁴⁹ Fe₂O₃ nanoparticle–poly(ethylene oxide)-*b*-poly(isobutylene),³⁰ and Fe₃O₄ nanoparticle–stearic acid²⁰ blends have been studied. To our knowledge, this is the first time this concept has been applied to Langmuir films at an air–ethylene glycol interface.

PS-*b*-PEO consists of a hydrophobic polystyrene block and a hydrophilic poly(ethylene oxide) block, and it is known to form Langmuir films at the air–water interface. The morphology of the resulting PS-*b*-PEO film is strongly dependent on the relative length of the PS and PEO blocks^{50–52} and of the polymer concentration in the spreading dispersion.^{51,53} Therefore, these parameters were carefully chosen for this work. The best films were obtained with PS-*b*-PEO ($M_n = 38\,200$ g/mol) with 22 mass % of PEO in mixtures in which the mass ratio $m(\text{Co}):m(\text{PS-}b\text{-PEO})$ was 20:1. If the proportion of PS-*b*-PEO in the mixture was increased, the homogeneity of the film decreased.

Before mixing PS-*b*-PEO into the Co nanoparticle dispersion, we prepared a film of pure PS-*b*-PEO at the air–ethylene glycol interface. The corresponding surface pressure isotherm, the TEM image of the LS film, and the molecular structure of PS-*b*-PEO are shown in Figure 5. Small circular aggregates are observed in the PS-*b*-PEO film, showing that the PEO spreads on ethylene glycol and the hydrophobic PS forms aggregates. This is consistent with the conclusion drawn by Baker et al.⁵¹ about PS-*b*-PEO films at

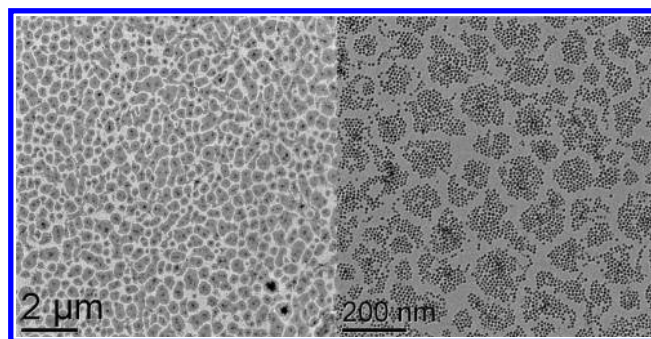


Figure 6. TEM image of Co(9.5 nm) nanoparticle/PS-*b*-PEO (38.2 K, 22 mass % of PEO) LS film with a mass ratio of 20:1. The film was deposited on ethylene glycol and transferred on the TEM grid at a mean particle area of 120 nm².

an air–water interface according to which in films with more than 10 mass % of PEO PS aggregates as isolated dot shaped domains.

We could visually observe that mixtures of Co nanoparticles and PS-*b*-PEO polymer spread more homogeneously on the ethylene glycol surface than the corresponding dispersions without PS-*b*-PEO. The TEM image of Co nanoparticle/PS-*b*-PEO film is shown in Figure 6. It can be observed that Co nanoparticles are arranged in domains in the estimated size range of 10 000 nm² that are separated from each other by a distance of approximately 10–50 nm.

We measured magnetic properties of these Co nanoparticle/PS-*b*-PEO films (in Figure 6) at 293 K and obtained an approximate saturation magnetism of 100 emu/g for cobalt (Figure S6a, Supporting Information). Sachan et al.²¹ have measured a saturation magnetization value of 105 emu/g at 10 K for LS films of oleic acid-protected Co nanoparticles 8 nm in diameter, which agrees well with our results. For bulk cobalt, the saturation magnetization value is 161 emu/g at room temperature.⁴² No coercivity was observed at 293 K, as expected for particles in this size range, indicating that the particles were superparamagnetic. At 2 K hysteresis corresponding to a small coercivity of ~30 Oe was observed (Figure S6b in the Supporting Information). This preliminary magnetic study indicated that the TDA-stabilized Co nanoparticles resist oxidation during the washing and LS procedures, which is consistent with the oxidation studies that show that TDA gives the Co nanoparticles good protection against oxidation (see Supporting Information section S1). After a rapid initial oxidation of the surface layer of the particle, oxidation slows down markedly as also predicted by the Cabrera–Mott model. Further oxidation is very slow compared to the time scale of the experiment. A systematic study of the magnetic properties of the Co nanoparticle/PS-*b*-PEO films (Figure 6) and of the interesting Co nanoparticle necklace structures with dipolar raft–raft interactions (Figures 4A,B) will be the subject for future work.

4. Conclusions

In this work, tridodecylamine (TDA)-stabilized Co nanoparticles (8.8 and 9.5 nm in diameter) were used for LS film preparation. Ethylene glycol was used as the subphase because it provided better spreading of the Co nanoparticles than water. The resulting films were characterized by Brewster angle microscopy (BAM), transmission electron microscopy (TEM), and SQUID magnetometer.

Various experimental LS factors were tested, including the nature of the subphase, solvent of the nanoparticle solution, and the presence of free TDA ligands and PS-*b*-PEO polymer in the

(47) Li, B.; Esker, A. R. *Langmuir* **2007**, *23*, 574–581.
 (48) Hottle, J. R.; Deng, J.; Kim, H.-J.; Farmer-Creely, C. E.; Viers, B. D.; Esker, A. R. *Langmuir* **2005**, *21*, 2250–2259.
 (49) Cheyne, R. B.; Moffitt, M. G. *Macromolecules* **2007**, *40*, 2046–2057.
 (50) Cox, J. K.; Yu, K.; Constantine, B.; Eisenberg, A.; Lennox, R. B. *Langmuir* **1999**, *15*, 7714–7718.
 (51) Baker, S. M.; Leach, K. A.; Devereaux, C. E.; Gragson, D. E. *Macromolecules* **2000**, *33*, 5432–5436.
 (52) Devereaux, C. A.; Baker, S. M. *Macromolecules* **2002**, *35*, 1921–1927.
 (53) Cheyne, R. B.; Moffitt, M. G. *Langmuir* **2005**, *21*, 5453–5460.

nanoparticle dispersion. The film formation was very sensitive to the experimental conditions; for example, the solvent (hexane or toluene) affected significantly the structure of the film. The nonamphiphilic nanoparticles are not surface-active so the traditional theories of Langmuir film formation and treatments of the surface pressure curves are not valid. In this work we observed that surface pressure–area isotherms provide very little information on the floating Co nanoparticle film and that BAM was needed to characterize the film formation *in situ*.

The removal of excess TDA ligands by washing the Co nanoparticle synthesis solution with 2-propanol prior to LS preparation and the addition of PS-*b*-PEO in the deposition dispersion were essential to obtain homogeneous films with high surface coverage. Best films were obtained with a mass ratio of 20:1 between Co (9.5 nm) and PS-*b*-PEO (38 200 g/mol, PEO content of 22 mass %). The saturation magnetization M_s of these films was 100 emu/g (293 K). When compared to M_s of bulk cobalt, 161 emu/g, it can be concluded that the Co(9.5 nm)/PS-*b*-PEO LS films are magnetically rather active; thus, the Co nanoparticles are not totally oxidized during the washing and LS procedures. Hysteresis curves measured at 293 K showed superparamagnetic behavior whereas at 2 K hysteresis with a small coercivity of ~ 30 Oe was observed.

Our work indicates that it is possible to obtain superparamagnetic LS films of Co nanoparticles that have an organic shell containing only bulky tridodecylamine molecules without any carboxylic acid molecules. In many applications the organic shell plays a vital role, and the use of other molecules than carboxylic acids may be required. TDA molecules are especially interesting ligands as they provide the Co nanoparticles a good protection against oxidation.

Acknowledgment. The financial support of Nokia Research Center, TEKES, OMG, and OUTOTEC is gratefully acknowledged. This work made use of the Nanomicroscopy Center (Aalto University).

Supporting Information Available: TEM images of non-washed and washed (ethanol, 2-propanol) tridodecylamine-stabilized Co nanoparticles, surface pressure–area isotherms of tridodecylamine on water and on ethylene glycol subphases, BAM images of floating Langmuir tridodecylamine film on ethylene glycol subphase, and magnetization curves of Co(9.5 nm) nanoparticle/PS-*b*-PEO (38.2 K, 22 mass % of PEO) LS film with a mass ratio of 20:1 at 293 and 2 K. This material is available free of charge via the Internet at <http://pubs.acs.org>.